The Astrophysical Journal, 831:184 (11pp), 2016 November 10 doi:10.3847/0004-637X/831/2/184

NEUTRON STAR MASS–RADIUS CONSTRAINTS OF THE QUIESCENT LOW-MASS X-RAY BINARIES X7 AND X5 IN THE GLOBULAR CLUSTER 47 TUC

Slavko Bogdanov[1], Craig O. Heinke[2], Feryal Özel[3], and Tolga Güver[4]
[1] Columbia Astrophysics Laboratory, Columbia University, 550 West 120th Street, New York, NY 10027, USA
[2] Department of Physics, University of Alberta, CCIS 4-183, Edmonton AB T6G 2E1, Canada
[3] Department of Astronomy, University of Arizona, 933 North Cherry Avenue, Tucson, AZ 85721, USA
[4] Istanbul University, Science Faculty, Department of Astronomy and Space Sciences, Beyazit, 34119, Istanbul, Turkey
Received 2016 March 4; revised 2016 August 9; accepted 2016 August 18; published 2016 November 7

ABSTRACT

We present *Chandra*/ACIS-S subarray observations of the quiescent neutron star (NS) low-mass X-ray binaries X7 and X5 in the globular cluster 47 Tuc. The large reduction in photon pile-up compared to previous deep exposures enables a substantial improvement in the spectroscopic determination of the NS radius and mass of these NSs. Modeling the thermal emission from the NS surface with a non-magnetized hydrogen atmosphere and accounting for numerous sources of uncertainties, we obtain for the NS in X7 a radius of $R = 11.1^{+0.8}_{-0.7}$ km for an assumed stellar mass of $M = 1.4\ M_{\odot}$ (68% confidence level). We argue, based on astrophysical grounds, that the presence of a He atmosphere is unlikely for this source. Due to the excision of data affected by eclipses and variable absorption, the quiescent low-mass X-ray binary X5 provides less stringent constraints, leading to a radius of $R = 9.6^{+0.9}_{-1.1}$ km, assuming a hydrogen atmosphere and a mass of $M = 1.4\ M_{\odot}$. When combined with all existing spectroscopic radius measurements from other quiescent low-mass X-ray binaries and Type I X-ray bursts, these measurements strongly favor radii in the 9.9–11.2 km range for a $\sim$1.5 $M_{\odot}$ NS and point to a dense matter equation of state that is somewhat softer than the nucleonic ones that are consistent with laboratory experiments at low densities.

Key words: dense matter – equation of state – globular clusters: individual (47 Tucanae) – stars: neutron

1. INTRODUCTION

The equation of state (EoS) of cold, stable matter at densities that exceed the nuclear saturation density ($\rho_{\rm sat} = 2.8 \times 10^{14}$ g cm^{-3}) remains one of the principal outstanding problems in nuclear physics. Neutron stars (NSs) provide a unique setting where the properties of neutron-rich matter at extreme conditions can be probed. This is because the mass–radius (*M*-*R*) relation of NSs is determined by the dense matter EoS and, in turn, measuring the mass *M* and radius *R* of several NSs with <10% errors can place strong limits on the EoS at high densities (see, e.g., Özel et al. 2010; Steiner et al. 2010).

It is well established that observing thermal radiation from the surface of an NS can serve as a useful tool toward this end. For an NS radiating uniformly from its entire surface, one can derive constraints on its mass and radius by fitting its spectrum with an appropriate atmosphere model—when the surface composition is known or can be determined from the X-ray spectrum itself—and combining the spectroscopic measurements with the distance to the source. Low magnetic field ($\ll 10^{10}$ G) sources are typically chosen for such studies so that the radiation transport or temperature distribution on the stellar surface are not affected by the magnetic field (see reviews by Özel 2013; Potekhin 2014). These criteria are met in quiescent low-mass X-ray binaries (qLMXBs) containing NSs and, in particular, for those located in globular clusters, to which the distances are well constrained (Rutledge et al. 2002). In these systems, the heat stored in the NSs is believed to be deposited by nuclear fusion in the deep crust during accretion, and is reradiated from the whole surface when accretion ceases, producing a long-lived thermal glow (Brown et al. 1998; Campana et al. 1998). Because qLMXBs have primarily thermal spectra and likely possess low magnetic fields ($\sim 10^{8-9}$ G), they can serve as fairly clean laboratories for studies of fundamental NS physics. As such, they can provide potentially strong constraints on NS structure that are complementary to those obtained using other techniques.

The observed thermal X-ray radiation from qLMXBs is modeled by light-element atmospheres because the lightest element that is present floats to the top of the atmosphere due to rapid gravitational settling on NS surfaces. Light-element atmospheres shift the peak of the emitted radiation to higher energies compared to a Planck spectrum of the same effective temperature because of the strong dependence of free–free absorption on photon energy and the large temperature gradients in such atmospheres (Rajagopal & Romani 1996; Zavlin et al. 1996). By applying the non-magnetic NS hydrogen atmosphere models of Zavlin et al. (1996) to X-ray observations of qLMXBs, Rutledge et al. (1999, 2001a, 2001b) obtained the first broad constraints on their radii. These earlier analyses of X-ray spectra from NSs with hydrogen atmosphere models produced radius estimates that are in reasonable agreement with theoretical predictions. These findings motivated a host of subsequent observations primarily using *Chandra* and, to a lesser extent, *XMM-Newton*, in an attempt to place tighter constraints on the NS radius. The known qLMXBs in globular clusters, in particular, have been the subject of intensive studies, including X7 and X5 in 47 Tuc (Heinke et al. 2003, 2006), U24 in NGC 6397 (Guillot et al. 2011; Heinke et al. 2014), source 26 in M28 (Becker et al. 2003; Servillat et al. 2012), NGC 2808 (Webb & Barret 2007; Servillat et al. 2008), NGC 6304 (Guillot et al. 2009a, 2009b), M13 (Gendre et al. 2003; Webb & Barret 2007; Catuneanu et al. 2013), ω Centauri (Rutledge et al. 2002; Gendre et al. 2003; Heinke et al. 2014), and M30 (Lugger et al. 2007; Guillot & Rutledge 2014).

Radius constraints obtained for qLMXBs from the different analyses have been combined and used for constraining the NS EoS. Guillot et al. (2013) applied Bayesian analysis techniques on the data for five qLMXBs to place limits on the NS radius, assuming that the radius is independent of mass. In this study, a number of sources of measurement uncertainty were incorporated into the final constraints, but some systematic uncertainties were not explored (Heinke et al. 2014; Lattimer & Steiner 2014). These include the possibility of a helium instead of hydrogen atmosphere for a subset of the sources as well as the effects of the model used for the relative abundances of the intervening absorbing material on the derived radius constraints. In a subsequent study of six qLMXBs, including those from Guillot et al. (2013), Özel et al. (2016) carried out a uniform analysis of these sources, using new information (e.g., updated absorption model and source distances) and additional considerations (e.g., a He atmosphere model for one of the sources), and found good agreement between all measurements. Furthermore, combining the qLMXB measurements with the radius measurements obtained during thermonuclear bursts led to a combined NS radius of 10.1–11.1 km (95% confidence level (C.L.)) and to tight constraints on the dense matter EoS. This comprehensive study, however, excluded two of the earlier qLMXB radius constraints, namely those of X5 and X7 (Heinke et al. 2003, 2006) due to concerns in the quality of the spectral data in these earlier *Chandra* observations, as we describe below.

The globular cluster 47 Tuc (NGC 104) hosts X7 and X5, with the highest and second-highest X-ray flux at Earth of any qLMXB in a globular cluster, making them well-suited targets for NS EoS constraints. A 270 ks *Chandra* observation of 47 Tuc in 2002 (Heinke et al. 2005) produced a spectrum of X7 with a high number of counts, which allowed the first measurements on the mass and radius of this source (Heinke et al. 2006). Using the `nsatmos` hydrogen atmosphere model in `XSPEC`, for an assumed NS mass of 1.4 $M_{\odot}$, the stellar radius was constrained to be $14.5^{+1.8}_{-1.6}$ km (90% C.L.). However, because the 270 ks *Chandra*/ACIS-S exposure of 47 Tuc was obtained in full-frame mode with a read-out time of 3.2 s, X7 suffered from strong event pile-up.[5] This resulted in substantial degradation in the quality of the spectrum. Furthermore, an extra model component to account for pile-up was required when fitting the spectrum, with a pile-up parameter that was estimated to be 15% in the 2002 full-frame data set.

It is difficult to quantify the systematic uncertainty introduced into the radius measurement by pile-up for two reasons. First, even though the pile-up correction is theoretically sound and verified to give reasonable results, it is not as well calibrated as *Chandra*'s performance in the absence of pile-up, especially when the pile-up fraction is as high as 15% (Guillot et al. 2013). Second, the inferred radius is highly sensitive to the spectral shape, for which it is not possible to fully correct. In light of this, it is clear that minimizing pile-up is critical for obtaining reliable constraints on the NS *M-R* relation with qLMXBs.

X5, an X-ray binary that is viewed edge-on (Heinke et al. 2003), on the other hand, shows eclipses with an 8.7 hr period and irregular energy-dependent dipping. The hydrogen column density $N_{\rm H}$ to X5 was high and variable during the 2002 ACIS-S observations but less so during the 2000 ACIS-I observations. Although the 2005 HRC-S observation lacks the spectral resolution to discern spectral variability, the presence of the same variability pattern as the 2000 observations is suggestive of the same variable absorption. The accretion disk in X5 appears to precess, occasionally blocking the view of the NS, as it did in 2002. Therefore, a view of the NS free of eclipses, dipping, and variable absorption is necessary to obtain an improved *M-R* measurement for this target.

Here, we present new *Chandra*/ACIS-S subarray observations of X5 and X7, totaling 181 ks, optimized for NS EoS constraints via X-ray spectroscopy. We show that the data suffer minimally from pile-up in the new observations and lead to radius constraints that are significantly different from those of the earlier studies of X5 and X7. Furthermore, we show that the new radius measurements are in excellent agreement with those from other qLMXBs and thermonuclear bursters.

The paper is organized as follows. In Section 2 we describe the observations and data reduction procedure. In Section 3, we assess the relevance of a number of causes of measurement bias and error, while we present the results of our spectroscopic analysis in Section 4. In Section 5 we discuss the implications of our findings and offer conclusions in Section 6.

Table 1
Chandra ACIS Subarray Observations of 47 Tuc Used in this Study

Instrument	ObsID	Date (UT)	Array size	Exposure (ks)
ACIS-I	78	2000 Mar 16	1/4	3.9
ACIS-S	3384	2002 Sep 30	1/4	5.3
ACIS-S	3385	2002 Oct 01	1/4	5.3
ACIS-S	3386	2002 Oct 03	1/4	5.5
ACIS-S	3387	2002 Oct 11	1/4	5.7
ACIS-S	15747	2014 Sep 09	1/8	50.0
ACIS-S	15748	2014 Oct 02	1/8	16.2
ACIS-S	16527	2014 Sep 05	1/8	40.9
ACIS-S	16528	2015 Feb 02	1/8	40.3
ACIS-S	16529	2014 Sep 21	1/8	24.7
ACIS-S	17420	2014 Sep 30	1/8	9.1

2. OBSERVATIONS

For the analysis presented here, we focus on new *Chandra*/ACIS-S exposures totaling 181 ks that were acquired between 2014 September and 2015 February. The observations are summarized in Table 1. During the exposures, only the ACIS-S3 chip was active and was configured in a custom 1/8 subarray, which restricts the region of the CCD in which data are taken to 128 rows, starting at row 449 (inclusive). This 1/8 subarray affords a 0.4 s frame time, which dramatically reduces the pile-up fraction of moderately bright sources such as X7 and X5.

The data extraction was carried out using CIAO[6] (Fruscione et al. 2006) version 4.7 and the corresponding calibration database (CALDB 4.6.7). For each observation, the source counts were extracted from circular regions of radius 2.″5 centered on the `wavdetect`-derived positions of both X5 and X7, which enclose ≈95% of the total source energy. The background was obtained from a source-free region on the

[5] Pile-up occurs when two or more photons, arriving at the same detector pixel during one frame time, are erroneously identified as a single photon with the sum of the photon energies or else altogether discarded (Davis 2001). The result is a distortion of the intrinsic shape of the source spectrum.

[6] *Chandra* Interactive Analysis of Observations.

image. None of the observations exhibit instances of enhanced count rate such as the ones that may arise due to background flaring. The source spectra from the individual observations were generated using `specextract` and were co-added using the `combine_spectra` task in CIAO. Due to known spectral calibration issues with ACIS-S data around 0.4 keV, we restrict our spectroscopic analysis to energies $\geqslant$0.5 keV. The spectral data were grouped so as to ensure at least 40 and 120 photons per energy bin for X5 and X7, respectively.

Using the CIAO tool `pileup_map`, we determined that the highest count rates per frame were 0.029 and 0.025 for X7 and X5, respectively, corresponding to a pile-up level of $\approx$1%.[7] While there are archival subarray observations from 2000 and 2002, they were acquired in a 1/4 array size, which provides a 0.8 s read-out time and hence a higher pile-up fraction. Based on this and the short total exposure of these data (26 ks), we do not consider them in the spectral analysis used to derive the *M-R* constraints presented below. We do, however, make use of these observations to examine the long-term variability of X7.

3. SOURCES OF MEASUREMENT BIAS

In order to utilize qLMXBs as high-precision probes of NS structure, it is important to explore and quantify the effect of any instrument or modeling uncertainties on the desired NS *M-R* measurement. Following the investigations presented in Heinke et al. (2014), Özel et al. (2016), and Elshamouty et al. (2016), we examine in this section several potentially important sources of measurement uncertainty and bias that may affect the EoS constraints obtained for X7 and X5.

3.1. Variability

Rapid (seconds/hours) and long-term (~years) variability in qLMXBs is often taken as an indicator of ongoing low-level accretion onto the NS. In such an event, the assumptions of a steady-state, passively cooling atmosphere, a purely thermal flux from the surface, or a uniformly hot star may no longer be valid. Servillat et al. (2012) examined the variability in *Chandra*/ACIS-S data of the qLMXB in M28 and found no statistically significant flux changes. More recently, Walsh et al. (2015) and Bahramian et al. (2015) have evaluated the variability of the thermal emission from 9 and 12 qLMXBs, respectively (see also Heinke et al. 2006; Guillot et al. 2011; Heinke et al. 2014, for individual sources). For the seven qLMXBs with purely thermal spectra, there is no evidence for temperature variations over ~10 yr down to levels of 11%.

To check for rapid variability, we applied the Kolmogorov–Smironov and Kuiper's tests to the unbinned event lists from each of the six 1/8 subarray exposures. In all instances, there is no evidence for variability as the events are fully consistent with being drawn from a distribution with constant count rate. In addition, the spectroscopically derived temperatures from the six exposures are consistent with one another within 90% confidence, with the largest temperature difference between observations being less than 4%.

The multi-epoch and high-quality *Chandra*/ACIS data set of X7 spanning ~15 yr allows us to place substantially stricter limits on the variability of its thermal radiation using spectral fits to the 2014/2015 combined data, and to the 2000 and 2002 subarray data.[8] For the most stringent test, we kept all parameters fixed except for the temperature in 2014/2015 and 2000/2002, which were allowed to vary independently. We find that the temperatures are virtually identical; at 90% confidence there is no observable temperature variation greater than 0.9% between the 2000/2002 and 2014/2015 epochs. Testing the normalization (which would correspond to any change in the emitting area) instead, we place an upper limit of 4% to any change in normalization at 90% confidence.

In contrast, the thermal X-ray flux of X5 is highly variable on short timescales (minutes to hours). However, this variability appears not to be due to ongoing accretion but rather due to X5 being an edge-on system. This geometric configuration results in occultations of the NS and variable absorption by the gas associated with the residual accretion disk. As detailed in Section 4, this necessitates the excision of a large fraction of the data for X5 in order to recover the intrinsic steady flux from the NS. Additionally, due to disk precession, the NS was completely obscured during the deep 2002 exposures, making it difficult to fully assess the long-term variability of the thermal component for X5. These difficulties make X5 results less reliable than those for X7.

3.2. Additional Spectral Components

Another usual cause for concern for the measurements of the NS radius from spectra is the possibility of additional, fainter X-ray emission components that have not been taken into account in the spectral modeling. In several qLMXBs, including Aquila X-1 (Rutledge et al. 2002), Centaurus X-4 (Campana et al. 2000), CX1 in NGC 6440, and CX12 in Terzan 5 (Bahramian et al. 2015), the presence of a power-law component in the quiescent flux suggests ongoing accretion at a low rate[9] (e.g., Garcia et al. 2001). Alternatively, "contaminating" power-law emission may arise due to a rotation-powered pulsar wind turning on in quiescence (see, e.g., Campana et al. 1998; Jonker et al. 2004) or unidentified blended sources in the crowded globular cluster core (see Guillot et al. 2009a, 2011, for the qLMXBs NGC 6304 and NGC 6553). It is possible that such a component is present at a very low level in the seemingly purely thermal qLMXBs but may still skew the NS radius measurement significantly if it is not accounted for. In particular, as the presence of a power-law component would harden the spectrum so that a fit with a purely thermal model would produce a higher temperature and, therefore, *M-R* limits that are shifted toward lower radii.

Following a number of previous studies (see Wijnands et al. 2001; Heinke et al. 2006; Guillot et al. 2013; Özel et al. 2016), to test this scenario, we introduced an additional power-law component into the model fits. Figure 1 illustrates the maximum possible contribution of a power-law component to the model spectrum of X7 for photon indices in the range typical for quiescent LMXB power-laws, $\Gamma = 1.0$–2.0 (Campana et al. 1998; Cackett et al. 2010; Chakrabarty et al. 2014). The addition of a power law results in a difference

[7] Based on the "*Chandra* ABC Guide to Pileup"; see http://cxc.harvard.edu/ciao/download/doc/pileup_abc.pdf.

[8] Because the extensive (~800 ks) *Chandra* HRC-S data set provides no spectral information, it is not useful in this regard.

[9] The best evidence for accretion at low luminosities in NS low-mass X-ray binaries comes from the recent detection of accretion-powered pulsations with power-law spectra at quiescent levels ($\sim 10^{33}$ erg s^{-1}) in the nearby millisecond pulsars PSR J1023+0038 and XSS J12270–4859 (Archibald et al. 2015; Papitto et al. 2015).

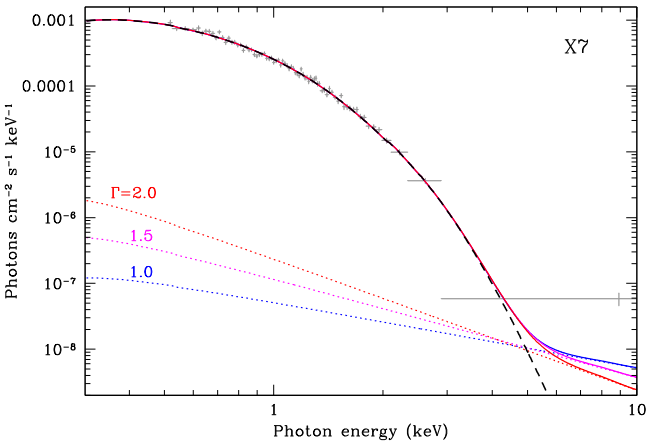

Figure 1. Best-fit models to the spectrum of X7 with the addition of a power-law component (dotted lines) with index 1.0 (blue), 1.5 (magenta), and 2.0 (red). The dashed line shows the best-fit model (`nsatmos`) for purely thermal hydrogen atmosphere emission. For reference, the unfolded *Chandra* subarray data of X7 fitted with a composite model of a H atmosphere plus power law with index 1.5 is show in light gray.

of 0.1% in the inferred nominal NS radius and its associated uncertainties, while the best fits with and without this component differ in χ^2_ν by a statistically insignificant 0.03. We found a similar result for X5, where the introduction of a power law causes a change of only 0.5% in the NS radius confidence limits. In both cases, the power-law normalization is consistent with zero within 1σ. For X7 and X5, we also derive upper limits of $\leqslant$0.2% and $\leqslant$1.6%, respectively, for any power-law component in the subarray spectra. We thus conclude that power-law emission is negligible for both of these qLMXBs and do not further consider a power-law component in the spectroscopic analyses that follow.

3.3. Chemical Composition of the Atmosphere

Given their transiently accreting nature, the thin atmospheric layer on the NSs found in qLMXBs most likely consists of the lightest element of the material supplied by the companion star. For a hydrogen-rich donor, due to gravitational settling, hydrogen is expected to surface within seconds and thus dominate the surface emission (Alcock & Illarionov 1980; Hameury et al. 1983; Brown et al. 2002).

For X5, the measured 8.7 hr orbit (Heinke et al. 2003) and the main-sequence-like optical counterpart (Edmonds et al. 2002) imply that the donor star is not a compact He star or C–O white dwarf and hence is hydrogen rich. Therefore, the NS almost certainly has a pure hydrogen atmosphere. In the case of X7, due to the lack of any information regarding the orbital period or the properties of the secondary star, the chemical composition of the accreted material is less certain. For example, this system may be an ultracompact binary (with an orbital period $\lesssim$80 minutes), in which case the companion star may be a helium star or a C–O core white dwarf that has surface layers (mostly) devoid of hydrogen (see, e.g., Nelemans & Jonker 2010). In light of this possibility, Servillat et al. (2012), Catuneanu et al. (2013), and Heinke et al. (2014) have considered He atmosphere fits to qLMXB spectra when there is no information about the nature of the companion. These fits produce larger inferred NS radii by up to $\approx$4–5 km for the same NS mass compared to H atmosphere models (e.g., Servillat et al. 2012; Catuneanu et al. 2013; Heinke et al. 2014), owing to the larger difference between the effective and color temperatures for He atmosphere emission. These results highlight the importance of the chemical composition of the NS surface layer on the NS M and R measurements.

Even in the case of an ultracompact binary and a hydrogen-poor companion, the question remains as to whether even trace amounts of hydrogen in the donor are sufficient to cover the NS surface with hydrogen. An optical depth of $\sim$unity can be achieved with a layer of hydrogen of thickness $\sim$1 cm on the NS surface, which requires only $\sim 10^{-20}\ M_\odot$ of H (see, e.g., Zavlin & Pavlov 2002 and Equation (20) of Özel 2013). As a result, even in the case of an ultracompact binary with accretion from a He-rich donor, minute abundances of H can still result in a hydrogen dominated atmosphere. An alternative means of accumulating a hydrogen atmosphere may be through nuclear spallation reactions of nuclei heavier than helium. However, it is not certain whether spallation always produces H during accretion (Bildsten et al. 1992, 1993). While H can be depleted from the photospheric layer via diffusive nuclear burning by an underlying layer of nuclei that are able to capture protons on timescales as short as 10^2–10^4 yr (see, e.g., Chang & Bildsten 2004; Chang et al. 2010), the atmosphere would likely fully replenish on much shorter timescales, even at very low accretion rates. Due to this ambiguity regarding the atmospheric composition, in Section 4 we present fits with both H and He atmospheres for X7.

3.4. Interstellar Absorption

Photoelectric absorption by the interstellar medium along the line of sight to the qLMXB significantly alters the intrinsic thermal spectrum of the NS, especially in the very soft X-ray band. Thus, as is the case for other variaties of NS systems (e.g., X-ray bursting sources), a reliable constraint on interstellar absorption is necessary for robust EoS constraints (see, e.g., Wroblewski et al. 2008; Lattimer & Steiner 2014). In addition to the total column density, the observed shape of the thermal spectrum is also sensitive to the chemical abundances of the intervening material. As a consequence, the inferred M-R constraints may differ based on the assumed ISM abundances. This is especially true for targets with large values of column density $N_{\rm H}$ since the absorption edges due to metals (whose depth depends on the relative abundances) become much more prominent.

The best estimate of $E(B-V) = 0.040 \pm 0.015$, combined with recent measurements indicating $N_{\rm H}/E(B-V) \approx 8.8 \times 10^{21}$ cm^{-2} (Bahramian et al. 2015; Foight et al. 2016), results in an exceptionally low absorbing column toward 47 Tuc, $N_{\rm H} = (3.5 \pm 1.5) \times 10^{20}$ cm^{-2} (assuming Wilms et al. 2000 abundances).

As demonstrated by Heinke et al. (2014), the strong sensitivity of the inferred NS radius on the choice of ISM abundances implies that low-$N_{\rm H}$ targets are best suited for the NS EoS constraints. In addition, the latest abundances and most complete absorption models that are appropriate for the ISM should be used in the spectral analyses. The currently best available abundances for the ISM (as opposed to values derived from the solar spectrum) is that of Wilms et al. (2000; `wilm` in XSPEC, incorporated into the absorption model *tbabs*), which we use in our analysis. Nevertheless, to test the sensitivity of the results on the absorption model, we also repeated the spectroscopic fits by implementing two other abundance models available in XSPEC: `aspl` (Asplund et al. 2009) and

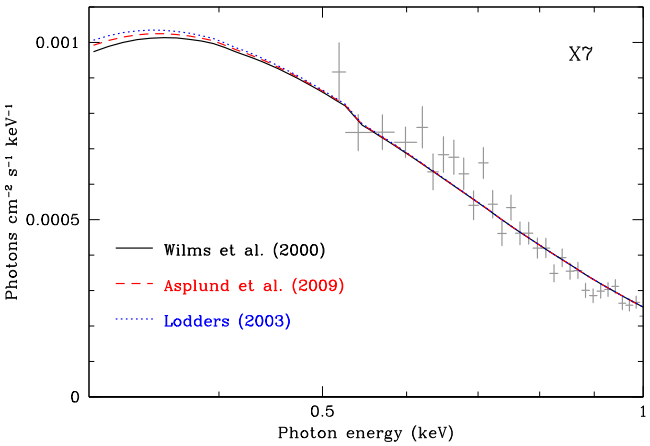

Figure 2. Best-fit absorbed hydrogen atmosphere (`nsatmos`) spectral model for X7 with three choices of interstellar absorption model: Wilms et al. (2000), Asplund et al. (2009), and Lodders (2003). Note the linear scale on the ordinate for the photon flux. The unfolded subarray data for X7 (light gray) fitted with an absorbed `nsatmos` model assuming Wilms abundances is shown for reference.

`lodd` (Lodders 2003), both of which are based on solar abundances.

As is evident from Figure 2, the choice of absorption model does not alter the model spectral shape above ∼0.5 keV due to the low absorbing column toward 47 Tuc. Therefore, using different abundance models has virtually no effect on the derived *M*-*R* relation. Specifically, for a fixed $M = 1.4\ M_{\odot}$, the best-fit value and associated uncertainties of R differ by less than 0.6% among the three abundance models. As shown below, for both X7 and X5 this level of uncertainty introduced by the choice of abundance model is dwarfed by the uncertainties due to instrument calibration.

3.5. Distance Uncertainty

Another important source of uncertainty in the radius measurements is the distance to the target qLMXB, which scales linearly with the NS radius at infinity. Globular cluster distances have been constrained using a variety of different methods, each of which has its own statistical and systematic errors (which may not always be well characterized). Fortunately, 47 Tuc has been a target for multiple distance investigations, giving us the opportunity to compare the results from multiple methods. In addition, the reddening to 47 Tuc is very small and well measured, nearly eliminating the concern about degeneracy between distance and reddening with measuring globular cluster distances.[10]

A compilation of 22 distance measurements to 47 Tuc, using seven general methods, is given in Table 1 of Woodley et al. (2012). The methods include the brightness of the horizontal branch, fitting an isochrone to the main sequence, cluster kinematics, RR Lyrae stars, the tip of the red giant branch, eclipsing binaries, and white dwarfs. We add to this list the recent white dwarf cooling sequence measurement of Hansen et al. (2013), which reports a distance modulus of $(m - M)_0 = 13.32 \pm 0.09$ magnitudes. Following Woodley et al. (2012), we calculated the weighted mean of all these estimates and the error in this mean to obtain a distance modulus of $(m - M)_0 = 13.31 \pm 0.02$, corresponding to a distance of $d = 4.59 \pm 0.04$ kpc. For this calculation, (i) we assumed errors of 0.20 mag for literature estimates without errors, (ii) we added statistical and systematic errors in quadrature, and (iii) we chose the estimate with binary corrections from the main-sequence fitting analyses of Gratton et al. (2003) and Carretta et al. (2000).

This analysis has several weaknesses. First, multiple measurements using the same method may lead to smaller statistical uncertainties but still contain a bias. Second, improvements in a method over time may not be reflected in the final calculation if all measurements are assigned equal weights. Finally, the final measurement could be significantly affected by results from a single flawed method. To address these, we select the subset of distance measurements since 2000, and also undertake a "jackknife" analysis, removing all measurements using one method to see how much the final result is affected. (For instance, removing all measurements that use white dwarfs, we find a distance modulus of 13.27 ± 0.02.) For all measurements since 2000, we find a distance modulus of $(m - M)_0 = 13.28 \pm 0.02$, or $d = 4.53 \pm 0.04$ kpc. Our jackknife tests on this subset find a range of best-fit distance moduli from 13.27 to 13.31, thus suggesting that systematic errors could affect the distance modulus by −0.01 or +0.03. Combining these jackknife-estimated errors with the error in the mean (±0.02) in quadrature, we arrive at a final range in distance modulus of 13.26–13.32, and a final distance estimate of $d = 4.53^{+0.08}_{-0.04}$ kpc. Alternative selections (e.g., jackknife tests on the full sample, or selecting only the most recent measurements using each method) arrive at consistent results.

We note that we excluded from our distance analysis the most recent measurement of Watkins et al. (2015), who obtained a significantly smaller dynamical distance for 47 Tuc ($d = 4.15 \pm 0.08$ kpc), compared to the mean value derived above. This is because we believe that this reported value is affected by problems in some of the radial velocity data used in that study. Dynamical distances are derived by comparing angular proper motions on the sky (typically from multiple *Hubble Space Telescope* epochs) with radial velocity dispersions of bright stars. The radial velocity measurements carried out by McLaughlin et al. (2006) and Lane et al. (2010) were of individual stars, but these studies did not check whether multiple stars might be blended together (as attempted by Gebhardt et al. 1995). Such blending tends to depress the line-of-sight velocity dispersion in the central regions. Indeed, such blending within the central ∼1′ can be verified by comparing the positions of stars used for radial velocities in 47 Tuc by McLaughlin et al. (2006) with the *HST* image provided in the same paper, and the radial velocity measurements within this central region show more scatter than elsewhere. Watkins et al. (2015) only used velocity dispersion information from the central regions (within <100″) for their primary analysis, to ensure that proper motions and radial velocity dispersions were compared within the same region. However, in an appendix, Watkins et al. (2015) show that including velocity dispersion information from the outer regions leads to a larger inferred distance of 4.61 ± 0.08 kpc. Thus, we have a plausible explanation for the discrepancy between the fiducial distance reported by Watkins et al. (2015), and the larger distance supported by photometric methods, and by the consideration of a larger radial velocity database.

[10] As discussed in Heinke et al. (2014), no individual method, not even cluster kinematics, is entirely free of systematic uncertainties.

3.6. Instrument Calibration Uncertainties

The spectroscopic *M-R* measurement technique using qLMXBs discussed herein relies on an absolute determination of the flux emitted from the NS. Because of this, it depends strongly on the reliability of the calibration of the instrument used for the measurement. Knowledge of the absolute effective area of the *Chandra*/ACIS detectors is limited by a combination of the uncertainties in the quantum efficiency near the read-out, the quantum efficiency non-uniformity across the detector resulting from charge transfer inefficiencies, and the depth of the contaminant on the ACIS filter (important primarily below ∼2 keV).

Following Guillot et al. (2013), we adopt a 3% systematic error to account for the instrument response uncertainties. We note that an in-depth evaluation of *Chandra* calibration uncertainties in the context of qLMXB NS *M-R* measurements based on the prescriptions by Drake et al. (2006), Lee et al. (2011), and Xu et al. (2014) will be presented in a subsequent publication.

3.7. Photon Pile-up

As noted previously, *Chandra*/ACIS data of even moderately bright sources are susceptible to severe event pile-up owing to the combination of slow read-out and high count rate. While we mitigated most of this negative effect in the new subarray observations by using a faster detector read-out mode, it still affects the data at a low level. The spectroscopic mass–radius measurement technique for qLMXBs is highly sensitive to the shape of the thermal spectrum. As a consequence, even a small artifical distortion in the spectral shape can bias the *M-R* measurement. For pile-up specifically, a portion of the photons piled at lower energies are either rejected entirely (if their event grades are consistent with those of cosmic rays) or recorded as a singe photon displaced to higher energies. As reported in Section 2, this occurs for ∼1% of the photons in the X7 and X5 spectra, which we would naively expect to be negligible.

To assess the impact of this seemingly small effect on our results, we repeated our spectroscopic fits with and without a pile-up model component (i.e., `pileup` in XSPEC). Figure 3 illustrates the results for X7, showing the 68% confidence contours in the *M-R* plane with and without pile-up. Despite the small degree of pile-up, the impact on the results is substantial. In addition to enlarging the confidence intervals, correcting for pile-up displaces them toward somewhat larger *M* and *R*. This arises because photon pile-up artificially hardens the intrinsic source spectrum, which produces a higher best-fit temperature and hence a smaller inferred stellar radius. The enlargement of the confidence contours arises principally from the statistical uncertainty in the pile-up parameter α, which gives the probability of rejection of piled events. In light of these findings, to ensure robust constraints on the NS *M* and *R*, pile-up correction should be incorporated into spectral modeling even for small (∼1%–2%) pile-up fractions.

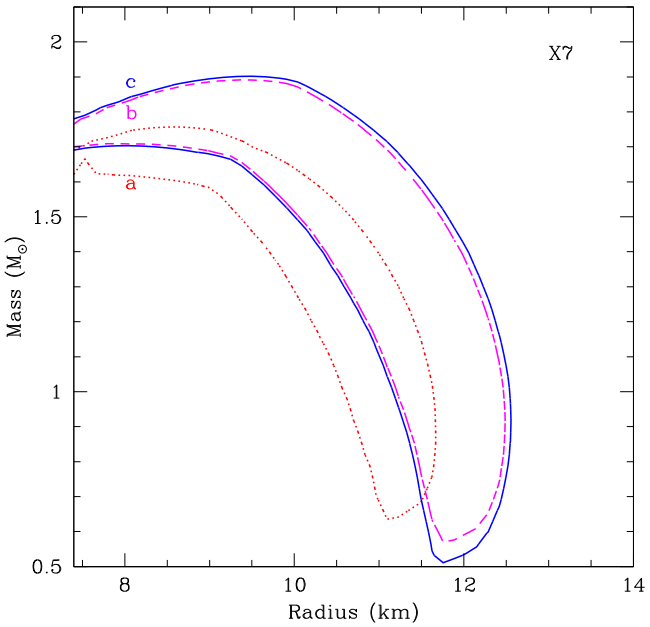

Figure 3. 68% confidence contours for the neutron star mass and radius obtained from fitting the spectrum of X7 with an absorbed H atmosphere model (`nsatmos`) with three different assumptions in the model: (a) no pile-up (red dotted line), (b) with pile-up (magenta dashed line), and (c) with pile-up and an additional 3% systematic uncertainty (blue solid line). Note the substantial displacement and enlargement of the contours when pile-up is introduced into the model.

4. RESULTS OF THE SPECTROSCOPIC ANALYSES

Having explored the various sources of formal and systematic errors, we performed the optimal spectroscopic fits in XSPEC using the `nsatmos` H atmosphere model (Heinke et al. 2006) for both X5 and X7 as well as the non-magnetic He atmosphere variant of the `nsx` additive table model (Ho & Heinke 2009) for X7. We also tested the `nsagrav` (Zavlin et al. 1996) H atmosphere model to identify any discrepancies in the measured radius and mass relative to `nsatmos`, which may arise due to differences between the numerical models used to construct them. The `nsatmos` and `nsagrav` models produce virtually identical results for the expected range of combinations of *M* and *R*. We chose the former in this analysis since it is defined over a larger range of *M* and *R*. To account for interstellar absorption and scattering, we used the `tbabs` model (Wilms et al. 2000). We further included the correction for the effect of pile-up, as discussed above. Thus, in what follows, we applied the multiplicative `pileup` model in XSPEC on the absorbed atmosphere model under consideration (i.e., `pileup*tbabs*nsatmos`). For the distance parameter in the `nsatmos` and `nsx` models, we restricted the allowed range of values to 4.49–4.61 kpc based on the discussion presented in Section 3.5. Finally, to incorporate the instrumental calibration uncertainty, we applied an additional 3% measurement error through the `systematic` command in XSPEC. The best-fit parameters for the various model for both X5 and X7 are summarized in Table 2.

In order to produce the final confidence contours for X5 and X7 and use a Bayesian approach to infer the NS EoS parameters from the *M-R* measurements, we first convert the χ^2 surfaces generated in XSPEC to a posterior likelihood over *M* and *R*. For this purpose, we take advantage of additional information, namely, that no plausible EoS models predict NSs with radii below ≈7 km and that stellar evolution is not expected to produce low-mass NSs with $\lesssim$0.5 $M_\odot$. Thus, we impose that for $R \leqslant 7$ km or $M \leqslant 0.5\ M_\odot$, the likelihood goes to zero.

Table 2
Summary of Mass–Radius Measurements for X7 and X5

Model[a]	$N_{\rm H}$[b] (10^{20} cm^{-2})	$kT_{\rm eff}$[c] (eV)	M ($M_\odot$)	R[d] (km)	χ^2/d.o.f.
		X5			
nsatmos	<4.9	236^{+18}_{-128}	$0.5^{+1.27}_{-0}$	$10.5^{+1.3}_{-10.5}$	95.1/88
	<5.2	225^{+26}_{-106}	(1.4)	$9.7^{+1.7}_{-2.0}$	95.2/89
	<5.0	121^{+134}_{-13}	$0.84^{+0.62}_{-0.35}$	(12)	96.6/89
		X7			
nsatmos	<2.2	120^{+129}_{-16}	$1.46^{+0.28}_{-1.46}$	$10.8^{+1.8}_{-10.8}$	88.2/70
	<2.3	120^{+114}_{-8}	(1.4)	$11.0^{+0.8}_{-0.7}$	88.2/71
	<2.3	110^{+5}_{-7}	$1.09^{+0.42}_{-1.09}$	(12)	88.7/71
nsx (He)	<3.3	91^{+92}_{-5}	$0.50^{+1.89}_{-0.50}$	$14.8^{+2.3}_{-0.6}$	82.9/70
	<3.3	102^{+3}_{-6}	(1.4)	$14.5^{+1.7}_{-0.9}$	83.0/71
	<3.3	103^{+81}_{-16}	$2.01^{+0.31}_{-0.16}$	(12)	83.2/71

Notes.
[a] All input models consider photon pile-up and a 3% systematic uncertainty.
[b] For $N_{\rm H}$, the lower bound in the fits was fixed to 1.3×10^{20} cm^{-2}. All fits reached this lower limit so only the 90% confidence upper bound is quoted.
[c] The values listed are redshift-corrected, i.e., as measured at the neutron star surface.
[d] All reported uncertainties correspond to 90% confidence level. Values in parentheses were held fixed during the fit.

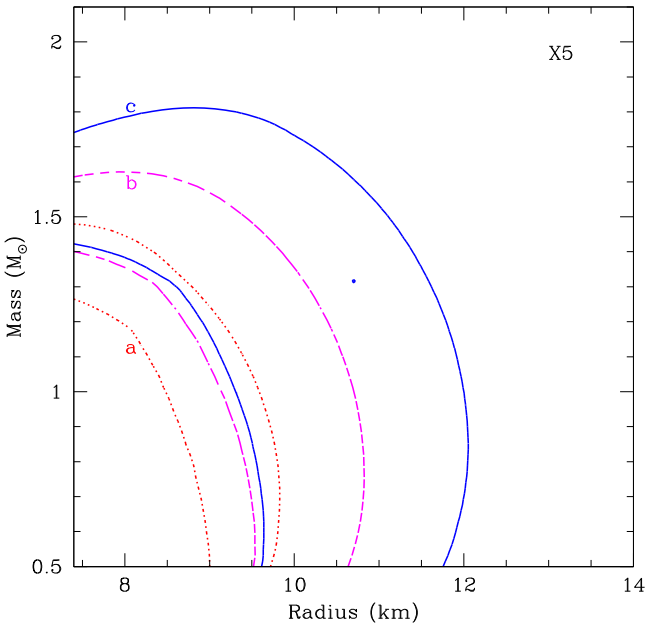

Figure 4. 68% confidence contours for the two parameters of interest, M and R, obtained from fitting the spectrum of X5 with an absorbed H atmosphere model (nsatmos) with different assumptions in the data selection and model: (a) only removing the eclipses and assuming no pile-up (dotted red line), (b) with eclipses removed and including pile-up but with no count rate cuts (magenta dashed line) and (c) with eclipses removed, pile-up included, and count rate cuts (solid blue line).

4.1. X5

The new 1/8 subarray *Chandra*/ACIS data set reveal that, for the majority of the time, the accretion disk does not completely obscure the NS in X5. However, during the two shortest exposures (ObsIDs 15748 and 17420) the system appears highly variable, possibly due to obscuration by the accretion disk. As already known from the 2000 and 2005 *Chandra* data, the system undergoes regular, deep eclipses every 8.666 hr as well as dips occurring ~2000 s prior to the main eclipse, which exhibit an enhancement in $N_{\rm H}$ (Heinke et al. 2003). Therefore, it is necessary to carefully excise the intervals in which X5 suffered eclipses and dips from our initial spectral analysis. To accomplish this, we extracted spectra using different time cuts around the eclipses and dips and fitted the spectra to check for any appreciable changes in the derived parameters. We show the results in Figure 4.

Throughout the orbit, X5 also exhibits rapid energy-dependent flux variability, with a spectral hardening at lower count rates. As our line of sight presumably grazes the accretion disk, this spectral variability is most likely due to absorption by material from the disk. It is evident from Figure 4 that the variable nature of X5 can result in skewed *M-R* measurements. In light of this, we took great care to excise the time intervals around the eclipses as well as the instances of energy-dependent decline in flux. For the latter, we determined that a conservative count rate cut of $\geqslant$0.07 cts s^{-1} (in the 0.3–4 keV range) removes the data strongly affected by absorption.

We show in Figure 5 the temporal and count rate cuts we applied to eliminate these portions of the data, which result in a 88.5 ks effective exposure. We show in Figure 6 the fitted X-ray continuum and in Figure 7 the resulting 68% and 95% confidence contours for the mass and radius of X5 using the filtered data. The results indicate an NS radius $R = 9.6^{+0.9}_{-1.1}$ km

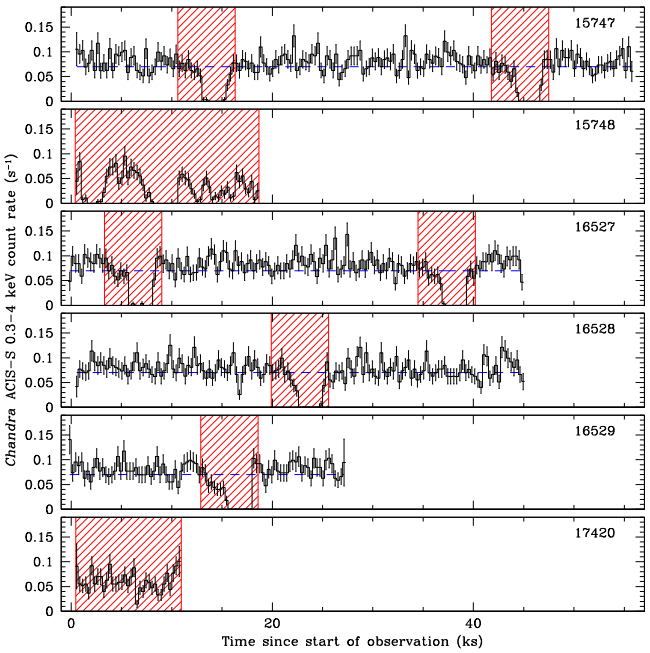

Figure 5. *Chandra*/ACIS-S subarray light curves of X5 in the 0.3–8 keV band. The hatched segments mark the time intervals excluded from the spectroscopic analysis due to eclipses or strong variability, while the horizontal dashed line marks the count rate cut, below which the remaining data were excised.

(at 68% C.L.) for an assumed mass of $M = 1.4\,M_\odot$, with $\chi^2_\nu = 1.07$ for 89 degrees of freedom. A radius of 12 km lies outside of the 68% confidence contour and the mass is constrained to $M < 1.3\,M_\odot$ for that radius at 95% confidence level. We note that the lower bound of the 68% confidence interval falls below $M = 0.5\,M_\odot$ where the nsatmos model

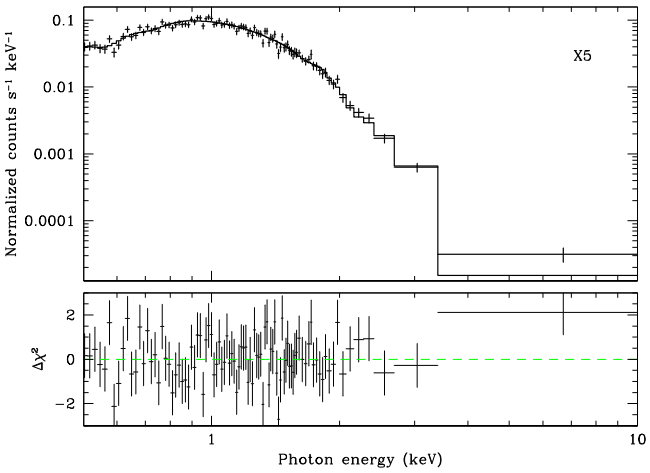

Figure 6. The total *Chandra*/ACIS-S subarray spectrum of X5 fitted with an absorbed H atmosphere model (`nsatmos`) convolved with a pile-up model (top) and the best-fit residuals (bottom).

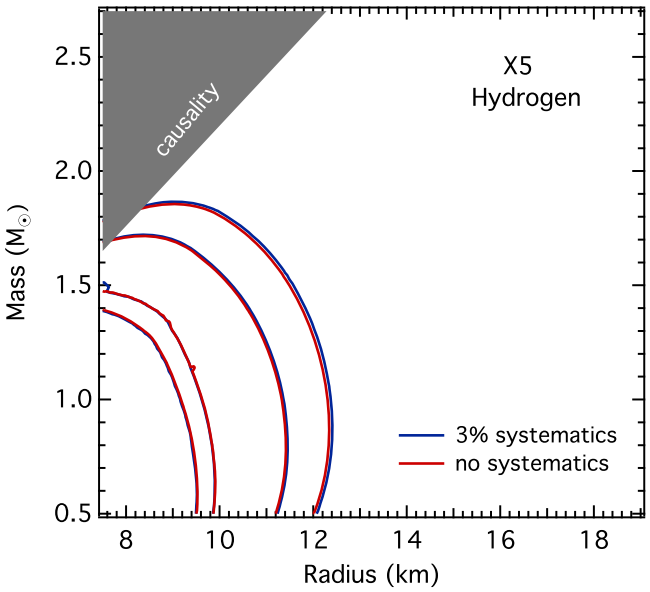

Figure 7. Mass–radius constraints obtained for X5 by fitting the *Chandra*/ACIS-S 1/8 subarray data with a piled-up and absorbed hydrogen atmosphere model (`nsatmos`). The 68% and 95% confidence levels are shown, obtained from the posterior likelihood over M and R (see text). The blue and red lines correspond, respectively, to the fits with and without a 3% systematic uncertainty instrumental calibration uncertainties. The shaded gray area in the upper left marks the region excluded by causality constraints. See Table 2 for best-fit parameters.

has not been calculated, since stellar evolution suggests that such low-mass NSs are not produced.

4.2. X7

We repeated the analysis described above for X7 and show in Figure 8 the total *Chandra*/ACIS-S 1/8 subarray spectrum as well as the best-fit H (`nsatmos`) and He (`nsx`) atmosphere models, which produce statistically similar fits (with χ^2_ν of 1.23 and 1.17, respectively). The resulting 68% and 95% confidence contours on the NS mass and radius for both models are shown in Figure 9. Assuming a H atmosphere and for $M = 1.4\ M_\odot$, we obtain a best-fit radius $R = 11.1^{+0.8}_{-0.7}$ km. For a He atmosphere, with the same fixed mass, the fit results in

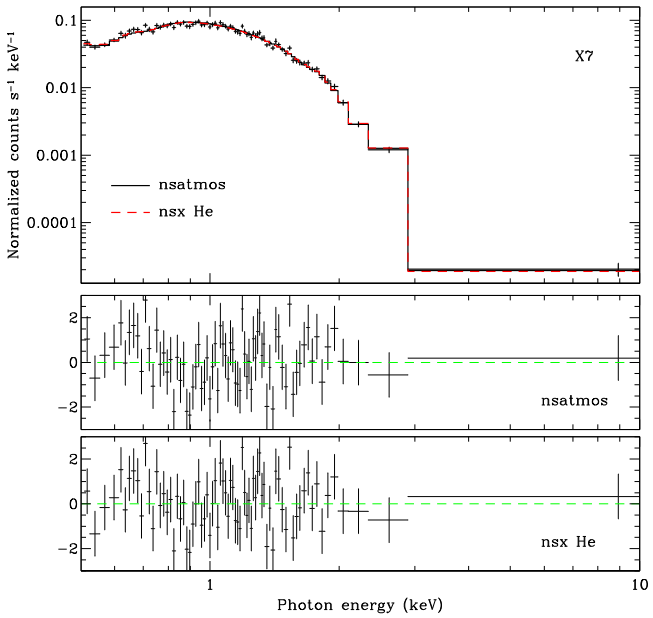

Figure 8. Total *Chandra* ACIS-S subarray spectrum of X7 fitted with an absorbed atmosphere model convolved with a pile-up model. The bottom panel shows the best-fit residuals expressed in terms of σ. Note that the fits with `nsatmos` and `nsx` exhibit the same residual structure and are virtually indistinguishable.

$R = 14.7^{+1.3}_{-0.9}$ km. If we instead hold the radius fixed at 12 km, the H atmosphere model results in a low NS mass with a best-fit value of $M = 1.1^{+0.3}_{-0.4}\ M_\odot$, while the He model favors a massive NS with $M = 2.1^{+0.2}_{-0.2}\ M_\odot$. All uncertainties quoted above correspond to a 68% confidence level.

4.2.1. X7: Hydrogen or Helium?

As noted previously, while there are numerous theoretical reasons to expect a hydrogen atmosphere, in the absence of any information regarding the orbital parameters and companion properties of X7, we cannot definitively determine whether the NS atmosphere is dominated by hydrogen or helium. However, there are some astrophysical arguments in favor of a lower-mass star and hence a H atmosphere.

Neutrino emission and cooling mechanisms, including direct URCA, hyperon URCA, and quark core cooling, all[11] depend strongly on the density of matter in the core, and thus on the NS mass. Thus, NSs that are very cold (compared to their known long-term rate of mass accretion) must be more massive than NSs that are relatively hot (for their mass accretion rate); see, e.g., Yakovlev & Pethick (2004) and Beznogov & Yakovlev (2015). The transiently accreting X-ray binary SAX J1808.4−3658 has a very cold NS, compared to what would be expected through "standard" cooling, whereas most other observed NSs in X-ray binaries are much warmer (see Heinke et al. 2007, 2009; Wijnands et al. 2013). The low temperature of SAX J1808.4−3658 suggests it has a higher mass than that of other quiescent NSs, with the latter presumably near the typical mass of 1.4 $M_\odot$. However, current evidence indicates that SAX J1808.4−3658 does not have a particularly high mass, with $M_{\rm NS} < 1.6\ M_\odot$ (at $\sim 2\sigma$; see Wang et al. 2013). In comparison, the relatively high and stable temperature of X7

[11] Except Cooper pair breaking and formation (Flowers et al. 1976), which is not relevant for this situation.

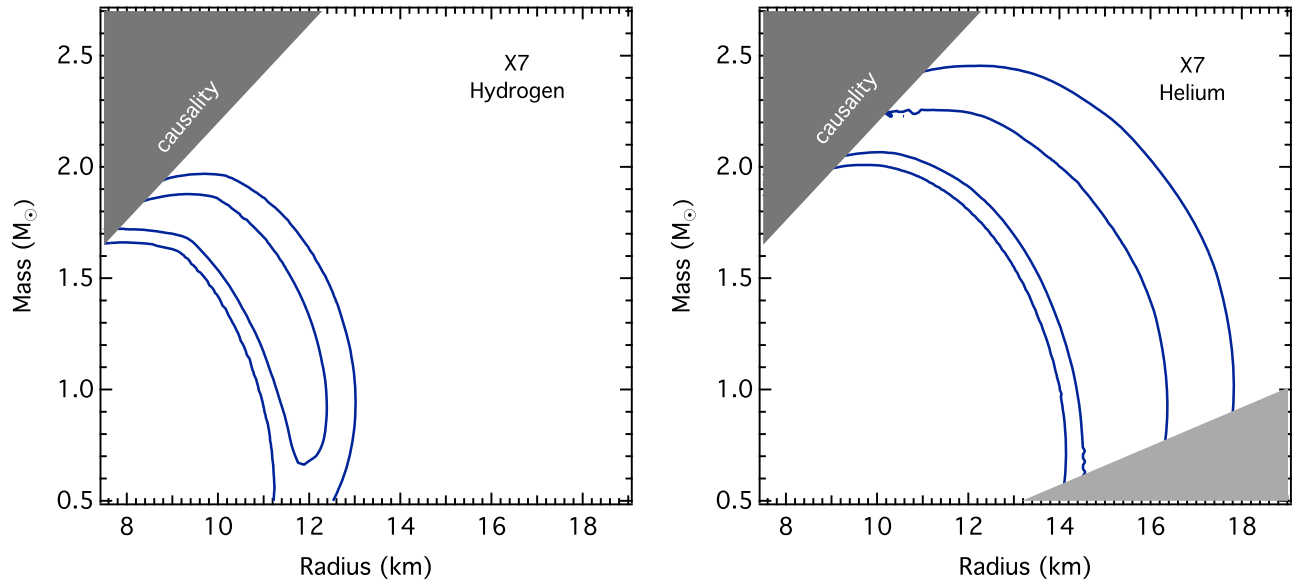

Figure 9. Mass–radius constraints obtained for X7 from the *Chandra*/ACIS-S subarray data assuming the `nsatmos` H atmosphere (top) and `nsx` He atmosphere (bottom) models. 68% and 95% confidence contours are shown obtained from the posterior likelihood over M and R (see text). For the He case, the light gray shading marks the region of the M-R space where the model atmospheres are not tabulated. A 3% systematic uncertainty in the calibration and a model for 1% pile-up are included in the analyses. See Table 2 for the best-fit parameters.

(which at $L_X = 1.5 \times 10^{33}$ erg s^{-1} has the highest thermal luminosity of any quiescent NS LMXB in a globular cluster; see Figure 1 in Heinke et al. 2003 or the luminosities in Table 4 of Guillot et al. 2009a) strongly indicates that it has a relatively low mass, i.e., around 1.4 $M_\odot$ or lighter. This is contrary to our He atmosphere fits, which yield $M > 1.7\ M_\odot$, or else quite large radii (see the right panel of Figure 9). Such a large mass should lead to rapid cooling of X7 to temperatures at least as low as that of SAX J1808.4−3658, contrary to observations.

We find that a He atmosphere model would require either a quite large radius or a high mass. A high mass would be at odds with our current understanding of cooling processes based on other qLMXBs, while a large radius (>14 km) would conflict both with the measurements of the radius of X5 presented here, and with measurements of other NSs (Guillot et al. 2011; Heinke et al. 2014; Özel et al. 2016), including the radius derived for the NS in NGC 6397 for either H or He atmospheres. Based on this line of reasoning, we argue that a hydrogen composition for the atmosphere of X7 is more plausible.

5. IMPLICATIONS FOR THE NS EoS

Most existing mass–radius measurements of NSs from a variety of methods have uncertainties that are too large to offer useful constraints when considered individually. Nevertheless, as shown recently in Özel et al. (2016), when taken as an ensemble, these results can produce fairly tight constraints on the EoS. We now add the M-R measurements of X7 and X5 to those used in the earlier study to infer the NS EoS.

To accomplish this, we make use of the Bayesian statistical framework developed in Özel et al. (2016) to measure the most likely dense matter EoS and the corresponding NS radii from all of the spectroscopic measurements. This framework makes use of parametric representations of the EoS and allows us to use these radius measurements to directly infer the pressures at several fiducial densities above the nuclear saturation density, i.e., at $\rho_1 = 1.85\ \rho_{\rm sat}$, $\rho_2 = 3.7\ \rho_{\rm sat}$, and $\rho_3 = 7.4\ \rho_{\rm sat}$ by exploiting the unique mapping between the pressure-density relation of cold supra-nuclear matter and the NS M-R relation (Lindblom 1992; Lattimer & Prakash 2001; Özel & Psaltis 2009; Read et al. 2009; Hebeler et al. 2010). This statistical inference also allows us to consider additional information and constraints on the dense matter EoS, such as the results of laboratory experiments in the vicinity of nuclear saturation density (see Tsang et al. 2012; Lattimer & Lim 2013, and references therein), the requirement for a $\geqslant 2\ M_\odot$ maximum NS mass (Demorest et al. 2010; Antoniadis et al. 2013; see, also, reviews by Lattimer 2011; Özel & Freire 2016), the physical conditions of stability and causality for the parametric EoS, as well as different priors on the pressures P_1, P_2, and P_3 at the fiducial densities (see Section 5 of Özel et al. 2016 for additional details).

Using this framework, we combine the radius likelihoods for X7 and X5 presented here with those of the 12 sources included in Özel et al. (2016) to infer the posterior likelihoods over the pressures at the three fiducial densities. In Figure 10, we show the mass–radius relation that corresponds to the most likely triplet of pressures that is derived from the combined likelihoods of the 14 sources as well as the priors on the EoS discussed above. Specifically, these include the hydrogen atmosphere results for X5 and X7, based on the arguments in Section 4.2.1, as well as the six NSs for which thermonuclear burst data have been used to infer M and R and the six qLMXBs analyzed in Özel et al. (2016). We also show in Figure 10 the ranges of mass–radius relations that correspond to the regions of the (P_1, P_2, P_3) parameter space in which the posterior likelihood is within $e^{-1/2}$ and e^{-1} of its highest value. For comparison, we include in this figure a small selection of proposed EoS with different compositions and calculation techniques (see Özel et al. 2016 for the acronyms and further details).

It is evident from this figure that the empirical EoS that is preferred by the current radius measurements is consistent with

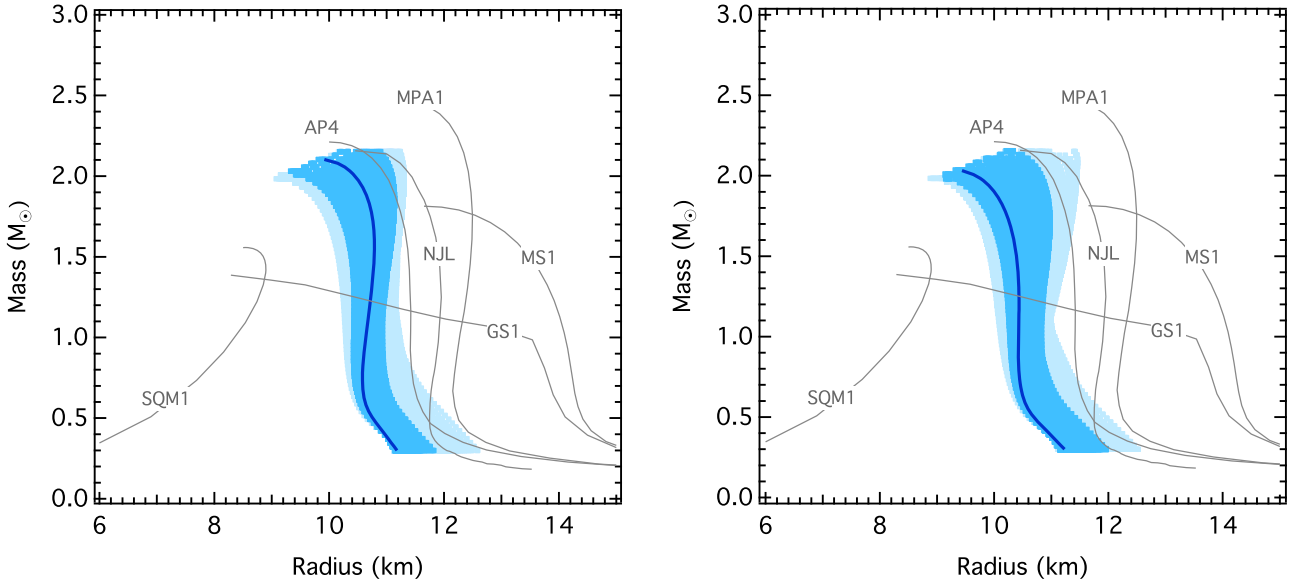

Figure 10. Mass–radius relation (solid blue curve) corresponding to the most likely triplet of pressures that agrees with the current neutron star data. These include the X5 and X7 radius measurements shown in this work, as well the neutron star radii measurements for the 12 neutron stars included in Özel et al. (2016), the low-energy nucleon–nucleon scattering data, and the requirement that the EoS allow for a $M > 1.97\ M_\odot$ neutron star. The ranges of mass–radius relations corresponding to the regions of the (P_1, P_2, P_3) parameter space in which the likelihood is within $e^{-1/2}$ and e^{-1} of its highest value are shown in dark and light blue bands, respectively. The results for both flat priors in P_1, P_2, and P_3 (top panel) and for flat priors the logarithms of these pressures (bottom panel) are shown.

relatively small radii. In particular, around 1.5 $M_\odot$, the 95% confidence range spans 9.9–11.2 km. This also indicates a fairly soft EoS; i.e., a lower pressure at and above 2 $\rho_{\rm sat}$ than those predicted by a number of nucleonic equations of state, such as AP4 (Akmal et al. 1998) shown in this figure.

6. CONCLUSIONS

We presented spectroscopically derived NS mass–radius constraints for the qLMXBs X5 and X7 in the globular cluster 47 Tuc based on new *Chandra* observations that were specifically optimized for this purpose. Although significantly shorter than the previous 270 ks ACIS-S full-frame exposure of 47 Tuc (Heinke et al. 2005), the 181 ks 1/8 subarray data of 47 Tuc we have presented here results in much tighter constraints on the *M-R* relation for X7. This is a direct consequence of the use of a faster read-out mode for the ACIS-S detector, which significantly reduced the pile-up fraction (from ∼15% to ∼1%) and, therefore, the distortion of the spectra due to the effects of pile-up. Furthermore, this substantially reduces the unquantified systematic uncertainties introduced by pile-up, which exibits non-linear behavior as a function of count rate and is not well calibrated. Indeed, the limits on M and R for X7 obtained in Heinke et al. (2006; see, in particular, their Figure 2) are only marginally consistent with those shown in Figure 9 using the same `nsatmos` H atmosphere model. This leads us to conclude that qLMXB data affected by a high pile-up fraction are not useful for reliable NS EoS constraints.

Another important finding of our evaluation of sources of measurement uncertainty described in Section 3 is that, even at a level of ∼1%, ignoring photon pile-up in the spectroscopic fits can lead to not only underestimated uncertainties but also a skewed measurement (as illustrated in Figures 3 and 4). This suggests that all previous qLMXB analyses that have not applied any necessary pile-up corrections in the spectroscopic fits should be re-examined. (Note that pile-up is well below 1% for a number of *Chandra* observations of qLMXBs and the previous analyses of the qLMXB in M28 take into account a pile-up correction for a ∼4% pile-up fraction in those data; see Guillot et al. 2013.)

Unlike most other globular cluster qLMXBs, the observed spectra of X7 and X5 are not strongly attenuated by photoelectric absorption from interstellar gas. As a result, the spectroscopic constraints we have obtained here do not suffer from appreciable uncertainties due to lack of information on the relative chemical abundances of the interstellar medium (see Heinke et al. 2014, for further details). When taken together with other factors, such as the well-determined distance to 47 Tuc, this makes the X7 radius measurements and the resulting NS EoS constraints presented here some of the most robust based on this spectrosopic technique.

The mass and radius constraints we find for X5 and X7 through these new observations are highly consistent with the 12 other spectroscopic radius measurements that have been performed to date for qLMXBs and thermonuclear bursters (see Özel et al. 2016). The increase in the radius measurements as well as the consistency of the results for different sources with a variety of different uncertainties increases our confidence in these measurements. Furthermore, it allows us to place increasingly tighter constraints on the dense matter EoS, especially when combined with other measurements, such as nuclear experiments near nuclear saturation density and the high NS masses measured through pulsar timing.

Indeed, by combining the results for X5 and X7 with existing *M-R* measurements from other qLMXB as well as bursting NSs, we obtain increasingly more robust constraints on the NS EoS. Specifically, we find that the preferred EoS that is empirically derived from the measurements of all 14 sources predicts radii between 9.9 and 11.2 km around $M = 1.5\ M_\odot$ (corresponding to the range where the likelihood falls to e^{-1} of its maximum value). This also implies a relatively low pressure around twice nuclear saturation density, which most directly affects NS radii. We find that such an EoS can easily produce

$\sim 2\ M_{\odot}$ NSs, which is observed through radio pulsar timing. This preferred EoS is softer than some purely nucleonic equations of state that are tuned to fit experiments at low densities, such as AP4, and may point to new degrees of freedom appearing around $\sim 2\ \rho_{\rm sat}$ in neutron-rich matter.

We thank W.C.G. Ho and S. Guillot for numerous helpful comments and discussions. This work was funded in part by NASA Chandra grants GO4-15029A and GO4-15029B awarded through Columbia University and the University of Arizona and issued by the Chandra X-ray Observatory Center, which is operated by the Smithsonian Astrophysical Observatory for and on behalf of NASA under contract NAS8-03060. C.O.H. acknowledges support from an NSERC Discovery Grant and a Humboldt Fellowship, and the hospitality of the Max Planck Institute for Radio Astronomy, Bonn, Germany. T. G. was supported by Scientific Research Project Coordination Unit of Istanbul University, Project numbers 49429 and 57321. This research has made extensive use of the NASA Astrophysics Data System (ADS), the arXiv, and software provided by the Chandra X-ray Center (CXC) in the application package CIAO.

Facility: CXO (ACIS).

REFERENCES

Akmal, A., Pandharipande, V. R., & Ravenhall, D. G. 1998, PhRvC, 58, 1804
Alcock, C., & Illarionov, A. 1980, ApJ, 235, 534
Antoniadis, J., Freire, P. C. C., Wex, N., et al. 2013, Sci, 340, 448
Archibald, A. M., Bogdanov, S., Patruno, A., et al. 2015, ApJ, 807, 62
Asplund, M., Grevesse, N., Sauval, A. J., & Scott, P. 2009, ARA&A, 47, 481
Bahramian, A., Heinke, C. O., Degenaar, N., et al. 2015, MNRAS, 452, 3475
Bauböck, M., Özel, F., Psaltis, D., & Morsink, S. M. 2015, ApJ, 799, 22
Becker, W., Swartz, D. A., Pavlov, G. G., et al. 2003, ApJ, 594, 798
Beznogov, M. V., & Yakovlev, D. G. 2015, MNRAS, 452, 540
Bildsten, L., Salpeter, E. E., & Wasserman, I. 1992, ApJ, 384, 143
Bildsten, L., Salpeter, E. E., & Wasserman, I. 1993, ApJ, 408, 615
Brown, E. F., Bildsten, L., & Chang, P. 2002, ApJ, 574, 920
Brown, E. F., Bildsten, L., & Rutledge, R. E. 1998, ApJL, 504, L95
Cackett, E. M., Brown, E. F., Miller, J. M., & Wijnands, R. 2010, ApJ, 720, 1325
Campana, S., Colpi, M., Mereghetti, S., Stella, L., & Tavani, M. 1998, A&ARv, 8, 279
Campana, S., Stella, L., Mereghetti, S., & Cremonesi, D. 2000, A&A, 358, 583
Carretta, E., Gratton, R. G., Clementini, G., & Fusi Pecci, F. 2000, ApJ, 533, 215
Catuneanu, A., Heinke, C. O., Sivakoff, G. R., Ho, W. C. G., & Servillat, M. 2013, ApJ, 764, 145
Chakrabarty, D., Tomsick, J. A., Grefenstette, B. W., et al. 2014, ApJ, 797, 92
Chang, P., & Bildsten, L. 2004, ApJ, 605, 830
Chang, P., Bildsten, L., & Arras, P. 2010, ApJ, 723, 719
Davis, J. E. 2001, ApJ, 562, 575
Demorest, P. B., Pennucci, T., Ransom, S. M., Roberts, M. S. E., & Hessels, J. W. T. 2010, Natur, 467, 1081
Drake, J. J., Ratzlaff, P., Kashyap, V., et al. 2006, Proc. SPIE, 6270, 1
Edmonds, P. D., Heinke, C. O., Grindlay, J. E., & Gilliland, R. L. 2002, ApJL, 564, L17
Elshamouty, K., Heinke, C., Morsink, S., Bogdanov, S., & Stevens, A. 2016, ApJ, 826, 162
Flowers, E., Ruderman, M., & Sutherland, P. 1976, ApJ, 205, 541
Foight, D., Guver, T., Özel, F., & Slane, P. 2016, ApJ, 826, 66
Fruscione, A., McDowell, J. C., Allen, G. E., et al. 2006, Proc. SPIE, 6270, 62701V
Garcia, M. R., McClintock, J. E., Narayan, R., et al. 2001, ApJL, 553, L47
Gebhardt, K., Pryor, C., Williams, T. B., & Hesser, J. E. 1995, AJ, 110, 1699
Gendre, B., Barret, D., & Webb, N. 2003, A&A, 403, L11
Gendre, B., Barret, D., & Webb, N. A. 2003, A&A, 400, 521
Gratton, R. G., Bragaglia, A., Carretta, E., et al. 2003, A&A, 408, 529
Guillot, S., Rutledge, R. E., Bildsten, L., et al. 2009a, MNRAS, 392, 665
Guillot, S., Rutledge, R. E., Brown, E. F., Pavlov, G. G., & Zavlin, V. E. 2009b, ApJ, 699, 1418
Guillot, S., Rutledge, R. E., & Brown, E. F. 2011, ApJ, 732, 88
Guillot, S., Servillat, M., Webb, N. A., & Rutledge, R. E. 2013, ApJ, 772, 7
Guillot, S., & Rutledge, R. E. 2014, ApJL, 796, L3
Haakonsen, C. B., Turner, M. L., Tacik, N. A., & Rutledge, R. E. 2012, ApJ, 749, 52
Hameury, J. M., Heyvaerts, J., & Bonazzola, S. 1983, A&A, 121, 259
Hansen, B. M. S., Kalirai, J. S., Anderson, J., et al. 2013, Natur, 500, 51
Hebeler, K., Lattimer, J. M., Pethick, C. J., & Schwenk, A. 2010, PhRvL, 105, 161102
Heinke, C. O., Grindlay, J. E., Lloyd, D. A., & Edmonds, P. D. 2003, ApJ, 598, 501
Heinke, C. O., Grindlay, J. E., Edmonds, P. D., et al. 2005, ApJ, 625, 796
Heinke, C. O., Rybicki, G. B., Narayan, R., & Grindlay, J. E. 2006, ApJ, 644, 1090
Heinke, C. O., Jonker, P. G., Wijnands, R., & Taam, R. E. 2007, ApJ, 660, 1424
Heinke, C. O., Jonker, P. G., Wijnands, R., Deloye, C. J., & Taam, R. E. 2009, ApJ, 691, 1035
Heinke, C. O., Cohn, H. N., Lugger, P. M., et al. 2014, MNRAS, 444, 443
Ho, W. C. G., & Heinke, C. O. 2009, Natur, 462, 71
Jonker, P. G., Galloway, D. K., McClintock, J. E., et al. 2004, MNRAS, 354, 666
Lane, R. R., Kiss, L. L., Lewis, G. F., et al. 2010, MNRAS, 401, 2521
Lattimer, J. M., & Lim, Y. 2013, ApJ, 771, 51
Lattimer, J. M. 2011, Ap&SS, 336, 67
Lattimer, J. M., & Prakash, M. 2001, ApJ, 550, 426
Lattimer, J. M., & Prakash, M. 2007, PhR, 442, 109
Lattimer, J. M., & Steiner, A. W. 2014, ApJ, 784, 123
Lee, H., Kashyap, V. L., van Dyk, D. A., et al. 2011, ApJ, 731, 126
Lindblom, L. 1992, ApJ, 398, 569
Lodders, K. 2003, ApJ, 591, 1220
Lugger, P. M., Cohn, H. N., Heinke, C. O., Grindlay, J. E., & Edmonds, P. D. 2007, ApJ, 657, 286
McLaughlin, D. E., Anderson, J., Meylan, G., et al. 2006, ApJS, 166, 249
Nelemans, G., & Jonker, P. G. 2010, NewAR, 54, 87
Özel, F. 2013, RPPh, 76, 016901
Özel, F., Baym, G., & Güver, T. 2010, PhRvD, 82, 101301
Özel, F., & Freire, P. 2016, ARA&A, 54, 401
Özel, F., & Psaltis, D. 2009, PhRvD, 80, 103003
Ozel, F., Psaltis, D., Guver, T., et al. 2016, ApJ, 820, 28
Papitto, A., de Martino, D., Belloni, T. M., et al. 2015, MNRAS, 449, L26
Potekhin, A. Y. 2014, PhyU, 57, 735
Rajagopal, M., & Romani, R. W. 1996, ApJ, 461, 327
Read, J. S., Lackey, B. D., Owen, B. J., & Friedman, J. L. 2009, PhRvD, 79, 124032
Rutledge, R. E., Bildsten, L., Brown, E. F., Pavlov, G. G., & Zavlin, V. E. 1999, ApJ, 514, 945
Rutledge, R. E., Bildsten, L., Brown, E. F., et al. 2001a, ApJ, 551, 921
Rutledge, R. E., Bildsten, L., Brown, E. F., et al. 2001b, ApJ, 559, 1054
Rutledge, R. E., Bildsten, L., Brown, E. F., Pavlov, G. G., & Zavlin, V. E. 2002, ApJ, 577, 346
Servillat, M., Webb, N. A., & Barret, D. 2008, A&A, 480, 397
Servillat, M., Heinke, C. O., Ho, W. C. G., et al. 2012, MNRAS, 423, 1556
Steiner, A. W., Lattimer, J. M., & Brown, E. F. 2010, ApJ, 722, 33
Tsang, M. B., Stone, J. R., & Camera, F. 2012, PhRvC, 86, 015803
Walsh, A. R., Cackett, E. M., & Bernardini, F. 2015, MNRAS, 449, 1238
Wang, Z., Breton, R. P., Heinke, C. O., Deloye, C. J., & Zhong, J. 2013, ApJ, 765, 151
Watkins, L. L., van der Marel, R. P., Bellini, A., & Anderson, J. 2015, ApJ, 812, 149
Webb, N. A., & Barret, D. 2007, ApJ, 671, 727
Wijnands, R., Degenaar, N., & Page, D. 2013, MNRAS, 432, 2366
Wijnands, R., Miller, J. M., Markwardt, C., Lewin, W. H. G., & van der Klis, M. 2001, ApJL, 560, L159
Wilms, J., Allen, A., & McCray, R. 2000, ApJ, 542, 914
Woodley, K. A., Goldsbury, R., Kalirai, J. S., et al. 2012, AJ, 143, 50
Wroblewski, P., Güver, T., & Özel, F. 2008, ApJ, submitted (arXiv:0810.0007)
Xu, J., van Dyk, D. A., Kashyap, V. L., et al. 2014, ApJ, 794, 97
Yakovlev, D. G., & Pethick, C. J. 2004, ARA&A, 42, 169
Zavlin, V. E., Pavlov, G. G., & Shibanov, Y. A. 1996, A&A, 315, 141
Zavlin, V. E., & Pavlov, G. G. 2002, in Neutron Stars, Pulsars, and Supernova Remnants, ed. W. Becker, H. Lesch, & J. Trümper (Max-Plank-Institut für extraterrestrische Physik: Garching bei München), 263